# Microstructure and Second-Phase Particles in Low- and High-Pressure Die-Cast Magnesium Alloy AM50

VAL Y. GERTSMAN, JIAN LI, SU XU, JAMES P. THOMSON, and MAHI SAHOO

The microstructure and phase composition of low-pressure die-cast (LPDC) and high-pressure die-cast (HPDC) magnesium alloy AM50 were examined by transmission electron microscopy (TEM) techniques in combination with optical microscopy, scanning electron microscopy (SEM), and electron-probe microanalysis (EPMA). It has been established that the dimensions and morphology of the constituent phases ($\alpha$-Mg solid solution, $Mg_{17}Al_{12}$, and $Al_8Mn_5$) depend on the processing parameters. The results obtained suggest that there is a ternary eutectic with the aforementioned three phases in the Mg-Al-Mn system. Phase transformations leading to the observed microstructures are discussed.

## I. INTRODUCTION

MAGNESIUM alloys have recently received considerable attention (*e.g.*, References 1 through 8 for recent international meetings). Their light weight makes them especially attractive to the automotive industry because their weight-reduction potential could, among other things, reduce greenhouse gas emissions. One such alloy is AM50, which has a good combination of castability and ductility. Both low-pressure and high-pressure die casting are being evaluated for production of automobile parts fabricated from this alloy. Low-pressure die casting is the process whereby the metal rises into the mold cavity against gravity using pressurized gas, and high-pressure die casting is the process in which the metal is forced into the mold cavity at a high speed and pressure.

There are several issues hindering the wider industrial application of die-cast Mg alloys, including poor ductility, low creep resistance, and susceptibility to stress-corrosion cracking. Properties of castings depend on the microstructure of the material; however, fundamental factors of microstructure formation and evolution during die casting are still not fully understood. Even though some limited microstructural studies have been performed on die-cast AM50 and similar alloys (*e.g.*, References 9 through 12), not all microstructural features have been positively identified and fully characterized. The main objective of this study was to comprehensively examine the microstructures and phase compositions of the low-pressure die-cast (LPDC) and high-pressure die-cast (HPDC) AM50 alloy. At the same time, the results obtained have allowed us to make some more general conclusions about the phase transformations in magnesium alloys containing aluminum and manganese, and a separate section of this article is devoted to that issue.

## II. EXPERIMENTAL

The chemical composition of the alloy AM50 samples examined in the present work is given in Table I. The LPDC samples were produced at CANMET-MTL, and the casting parameters were as follows: 725 °C casting temperature, 350 °C to 400 °C mold temperature, 2- to 3-second filling time, and 0.125 MPa filling pressure. The cooling rate for the LPDC samples was about 0.8 °C/s. The HPDC samples were cast at the Gibbs Die Casting Corporation (Henderson, KY), and the casting parameters were as follows: 7.6 m/s injection speed, 690 °C metal temperature, and 230 °C mold temperature. The cooling rate of the HPDC sample was estimated to be at least two orders of magnitude faster than that of the LPDC sample.

Metallographic samples were examined first with an optical microscope and then in a PHILIPS* XL30 scanning electron microscope equipped with an energy-dispersive X-ray spectrometer (EDS) and in a Cameca SX-51 electron-probe microanalyzer equipped with wavelength spectrometers.

Thin foils were prepared for transmission electron microscopy (TEM) by electropolishing disks cut from the middle of the casting bars. Some samples were then ion milled on both sides to remove the surface oxide layer. The samples were examined in a PHILIPS CM20 field-emission gun transmission electron microscope, and the chemical composition of the microstructural constituents was measured using an Oxford Instruments thin-window EDS detector with an INCA system analyzer.

## III. RESULTS AND DISCUSSION

### A. *Optical Microscopy, Scanning Electron Microscopy, and EPMA*

Figure 1 shows optical micrographs of as-cast LPDC and HPDC samples. Etching revealed both the dendrites and the grain boundaries. In the LPDC sample (Figure 1(a)), the grains are coarse (the mean linear-intercept grain size was 110 $\mu$m), and dendrites are visible within grains. The HPDC microstructure consists of grains of about one order of magnitude smaller than those of the LPDC microstructure. Grain boundaries in this sample are masked by the gray regions sometimes referred to as solidification cells (Figure 1(b)). Apparently, the network of these gray regions is a Mg matrix with a high Al concentration (supersaturated $\alpha$ solid solution),

*PHILIPS is a trademark of Philips Electronic Instruments Corp., Mahwah, NJ.

VAL Y. GERTSMAN, JIAN LI, and SU XU, Research Scientists, JAMES P. THOMSON, Research Engineer, and MAHI SAHOO, Program Manager, are with CANMET – Materials Technology Laboratory, Natural Resources Canada, Ottawa, ON, Canada K1A 0G1. Contact e-mail: vgertsma@nrcan.gr.ca

Manuscript submitted June 16, 2004.

**Table I. Chemical Composition of the Samples (Weight Percent)**

| Sample | Al | Mn | Si | Fe | Cu | Zn | Ni | Mg |
|---|---|---|---|---|---|---|---|---|
| LPDC | 5.0 | 0.27 | 0.018 | <0.0010 | 0.004 | 0.007 | 0.0010 | balance |
| HPDC | 4.9 | 0.34 | 0.024 | 0.0015 | 0.005 | 0.044 | 0.0021 | balance |

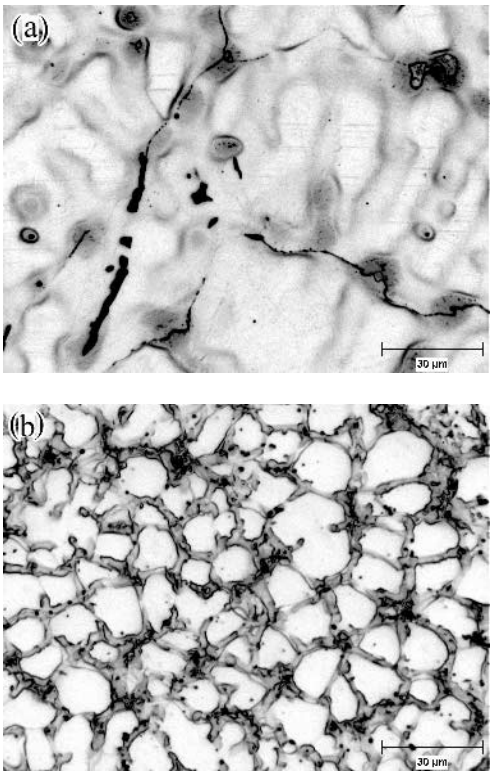


Fig. 1—Optical micrographs of the (*a*) LPDC and (*b*) HPDC samples.

as can be seen from the EPMA map (Figure 2); hence, they are somewhat similar to the interdendritic regions in the LPDC sample (compare Figures 3(a) and (c)). It is known that dendrite cores solidify first and contain a low concentration of Al. The concentration of aluminum (and other solutes) increases toward the dendrite periphery, and interdendritic areas become supersaturated. Supposedly, in the HPDC sample, solidification begins in the center of the cells, and, as the nucleus grows, its periphery becomes supersaturated with solutes. When crystals growing from different crystallization centers meet, grain boundaries between them should be in the middle of the supersaturated solid-solution bands. Therefore, grains should coincide with the casting cells, as was observed, *e.g.*, in a Mg-4 pct Al alloy.[13] However, in the present case, the grain boundaries do not completely coincide with the cell boundaries, as can be seen from Figures 2(a) and 3(d). This might be an indication that some postsolidification grain-boundary migration occurred during cooling. Nevertheless, the cell size is a good approximation of the grain size, and the mean value was 14 $\mu$m.

The EPMA and EDS analysis indicate that bright white spots visible on scanning electron microscopy (SEM) images (Figures 2 and 3) are inclusions of an Al-Mn phase. While some such inclusions are in the middle of grains, the majority of the Al-Mn particles are in the areas of supersaturated $\alpha$(Mg) solid solution. The larger and less bright spots are particles of an Al-Mg phase. Higher-magnification SEM images (Figures 3(b) and (d)) show that such particles actually represent two-phase mixtures. This could be an $\alpha$(Mg)-$\beta$($Mg_{17}Al_{12}$) eutectic. It should be noted that, under equilibrium conditions, alloy AM50 should not contain eutectic constituents, since the Al concentration is lower than the maximum solubility of Al in Mg at the eutectic temperature. Hence, the formation observed in the samples is actually nonequilibrium eutectic formed during fast cooling. These features are located within the areas of supersaturated solid solution. This suggests that, during solidification, the concentration of Al locally in the remaining liquid becomes so high that eutectic crystallization occurs. In the LPDC sample, many such formations are surrounded by very fine lamellar structures (Figure 3(b)), which is possibly another morphological form of the $\alpha$-$\beta$ phase mixture. As will be seen from the TEM results that follow, the origin of these structures may be different from the coarse eutectic constituents formed by crystallization from the melt.

### B. *The TEM Analysis*

There are no crystallographic boundaries between the areas of $\alpha$(Mg) solid solution with different solute contents. Therefore, areas such as dendrites in the LPDC sample and grain-periphery layers in the HPDC specimen cannot be distinguished by conventional TEM imaging techniques. In the latter case, as mentioned previously, there is no one-to-one correspondence between the cell-boundary layers and the grain boundaries. Hence, compositional EDS profiling across a grain boundary, similar to that reported in Reference 13, would not necessarily reveal enrichment in Al. However, random EDS sampling clearly shows a different Al concentration in the Mg matrix. The values measured within $\alpha$(Mg) grains ranged from 2.2 to 7.3 at. pct Al in the LPDC specimen and 3.4 to 8.9 at. pct Al in the HPDC specimen. This seems to reflect a faster cooling rate of the HPDC sample and, consequently, a less equilibrated concentration of Al, which should be below 3 pct at room temperature.[14,15,16] The manganese concentration in the matrix was, in most cases, below the EDS detection limit. According to the equilibrium Mg-Mn phase diagram,[14,15,16] there is almost no solubility of Mn in Mg at room temperature.

Secondary-phase particles of different sizes, shapes, and compositions were found in the samples. One phase was positively identified by electron diffraction and EDS as $Mg_{17}Al_{12}$ (Figures 4 and 5). This is an equilibrium phase in Mg-rich alloys, according to the Al-Mg phase diagram.[14,15,16] It has a complex cubic structure with a period of 1.056 nm. One of the observed morphological forms of this phase is the rounded eutectic constituent (Figures 4(a) and (b) and 5(a)). Islands of Mg matrix within such formations have an enhanced Al concentration (up to 9 pct). Usually, the $Mg_{17}Al_{12}$ eutectic constituents are single-crystalline (Figures 4(a) and 5(a)), although polycrystalline eutectic particles have also been observed occasionally (Figure 4(b)). Rounded eutectic constituents in the HPDC sample are, on average, smaller than those in the LPDC sample (*cf.* Figures 4(a) and 5(a)) and are encountered much less frequently. Besides this kind of $Mg_{17}Al_{12}$, large irregularly shaped $Mg_{17}Al_{12}$

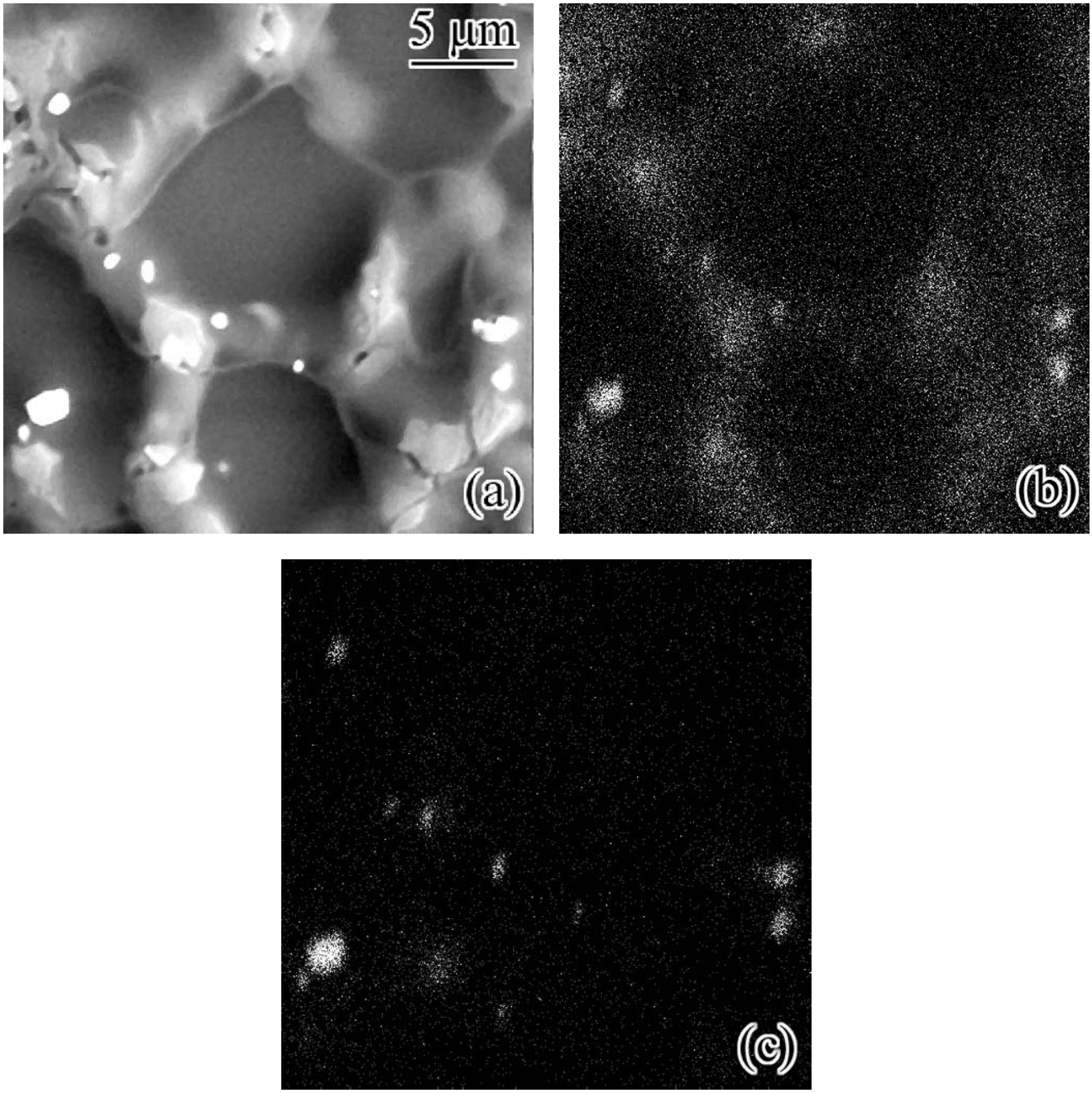


Fig. 2—EPMA chemical mapping of the HPDC sample: (*a*) secondary electron image, (*b*) Al, and (*c*) Mn.

particles could, on rare occasions, be found in the HPDC sample (Figure 5(b)). Apparently, this is a coarse eutectic constituent. Generally, our observations on the HPDC sample agree with the data of Sohn *et al.*,[10] that the $Mg_{17}Al_{12}$ phase was rarely observed in the die-cast AM50 alloy. Wang *et al.*[11] observed $Mg_{17}Al_{12}$ eutectic constituents in a different morphological form than in the present study—as lamellar structures. This is probably due to a different processing regime. On the other hand, microstructures observed around coarse eutectic particles, as in Figure 3(b), may be interpreted as lamellar eutectic constituents. Because of the very different spatial scales of the samples examined using TEM and SEM, the TEM specimen may contain one or another morphological form of the eutectic, depending on its specific location.

Much finer particles of $Mg_{17}Al_{12}$ were also found in the LPDC sample, some of which are shown in Figures 4(b) and (c). These are mostly elongated platelets or needle-shaped precipitates. Frequently, such precipitates surround rounded eutectic constituents, as seen in Figure 4(b). This may correspond to the SEM observations (Figure 3(b)) and may serve as an alternative explanation to the lamellar eutectic described previously. Apparently, these particles were formed by precipitation from the supersaturated solid solution during cooling. Such fine precipitates have never been observed in the as-cast HPDC specimen. However, it is

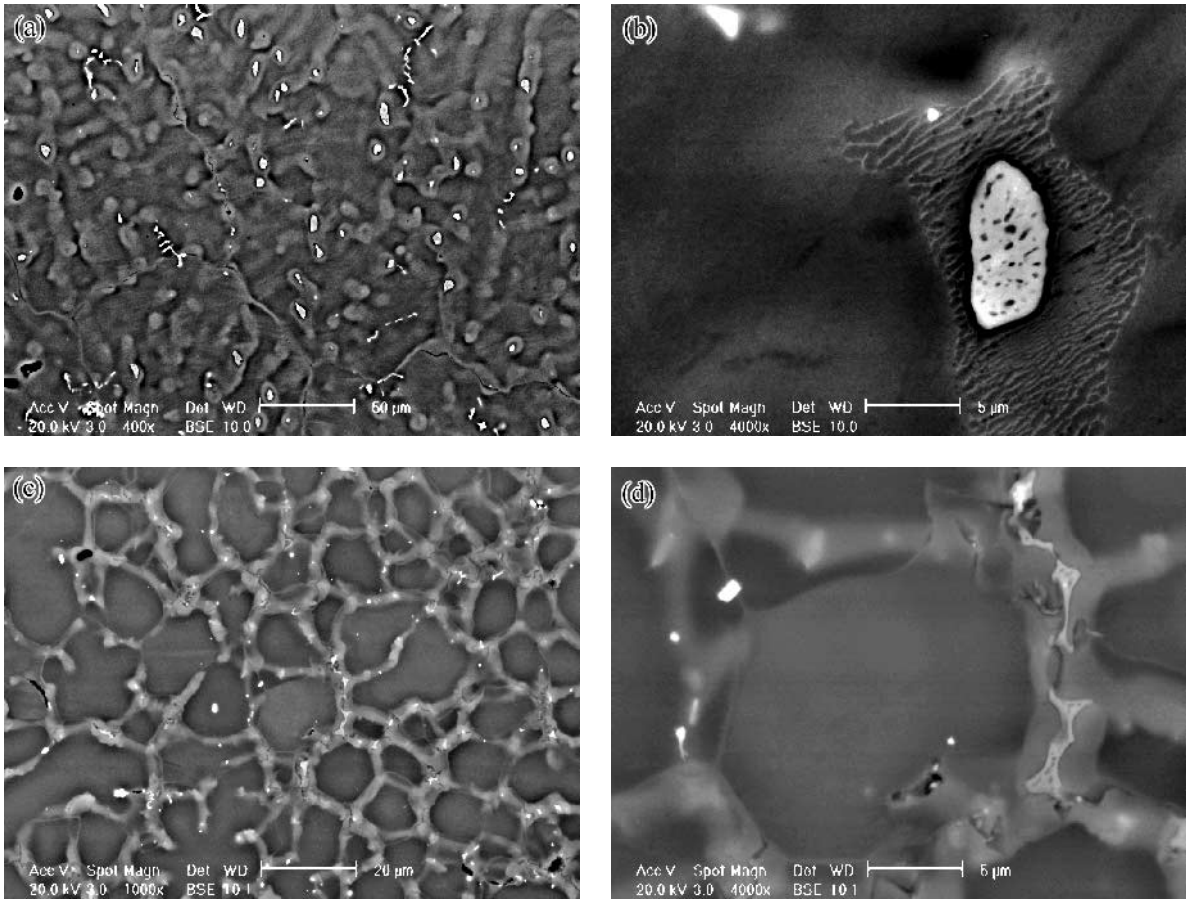


Fig. 3—Backscattered electron SEM images of the (*a*) and (*b*) LPDC and (*c*) and (*d*) HPDC samples.

noteworthy that the $Mg_{17}Al_{12}$ phase, including the fine elongated precipitates, is abundant in the HPDC sample after creep at elevated temperature[17,18] (Figure 6). This agrees with earlier observations[9,11,13] that both heating and deformation promote precipitation of this phase.

As can be seen in Figure 2, inclusions containing (Al + Mn) are also present in the die-cast AM50 alloy. Al-Mn intermetallic particles in die-cast Mg alloys have been observed by several researchers, but their identification is still uncertain. Sohn *et al.*[10] simply state that this is an intermetallic compound containing Al and Mn, whereas Wang *et al.*[11] identify the phase as $Al_8Mn_5$ having a hexagonal crystal structure with $a = 1.273$ nm and $c = 1.588$ nm. Actually, the equilibrium $Al_8Mn_5$ intermetallic has a rhombohedral structure with $a = 0.906$ nm and $\alpha = 89.3$ deg,[19] which, in trigonal coordinates, is described by $a = 1.265$ nm and $c = 1.586$ nm (*i.e.*, similar to the hexagonal description). This phase has a significant homogeneity range (~31 to 50 at. pct Mn).[14,15,16] In a recent study[12] on a similar alloy (AM60), a Mn-rich phase was identified by X-ray diffraction analysis as $Al_6Mn$. While the $Al_6Mn$ phase is quite common in Al-based alloys containing Mn, no reliable data have indicated its presence in any substantial amount in Mg alloys. Because of the uncertainty that exists with regard to the Al-Mn phase in Mg alloys, the results of this study will be presented in more detail.

Coarse Al-Mn inclusions were observed in both the LPDC and HPDC samples (Figure 7); the micrographs presented in this figure are typical in the sense that, in the LPDC sample, such particles are generally larger and are of irregular shape, whereas they often have crystal-like polyhedral shapes in the HPDC samples. However, EDS indicates a similar chemical composition of the particles in question in both samples: 60.7 ± 3.1 at. pct Al and 39.3 ± 3.1 at. pct Mn in the LPDC sample and 58.4 ± 7.0 at. pct Al and 41.6 ± 7.0 at. pct Mn in the HPDC sample. Thus, there is a very good agreement with the $Al_8Mn_5$ composition (the $Al_8Mn_5$ stoichiometry suggests 61.5 at. pct Al and 38.5 at. pct Mn), and the spread of individual measurements is within the homogeneity range for this phase (refer to the previous paragraph). Selected-area electron diffraction patterns from the particles could be indexed as $Al_8Mn_5$; Figure 8 shows an example of a diffraction pattern from a particle oriented such that the *c*-axis of the $Al_8Mn_5$ crystal lattice is parallel to the electron beam. High-resolution lattice imaging (Figure 9) confirms the Al-Mn phase identification as $Al_8Mn_5$.

Besides coarse $Al_8Mn_5$ particles, ultrafine precipitates containing Al and Mn were also present in some areas of the LPDC sample (Figure 10). It should be noted that Al-Mn particles with dimensions in the nanometer range have not been found in the HPDC samples. Because of the small precipitate dimensions, a considerable Mg peak is present on the EDS spectra due to through-thickness interaction of the electron beam with the alloy matrix, making direct quantitative analysis in this case meaningless. Nevertheless, quantitative compositional information could be extracted from

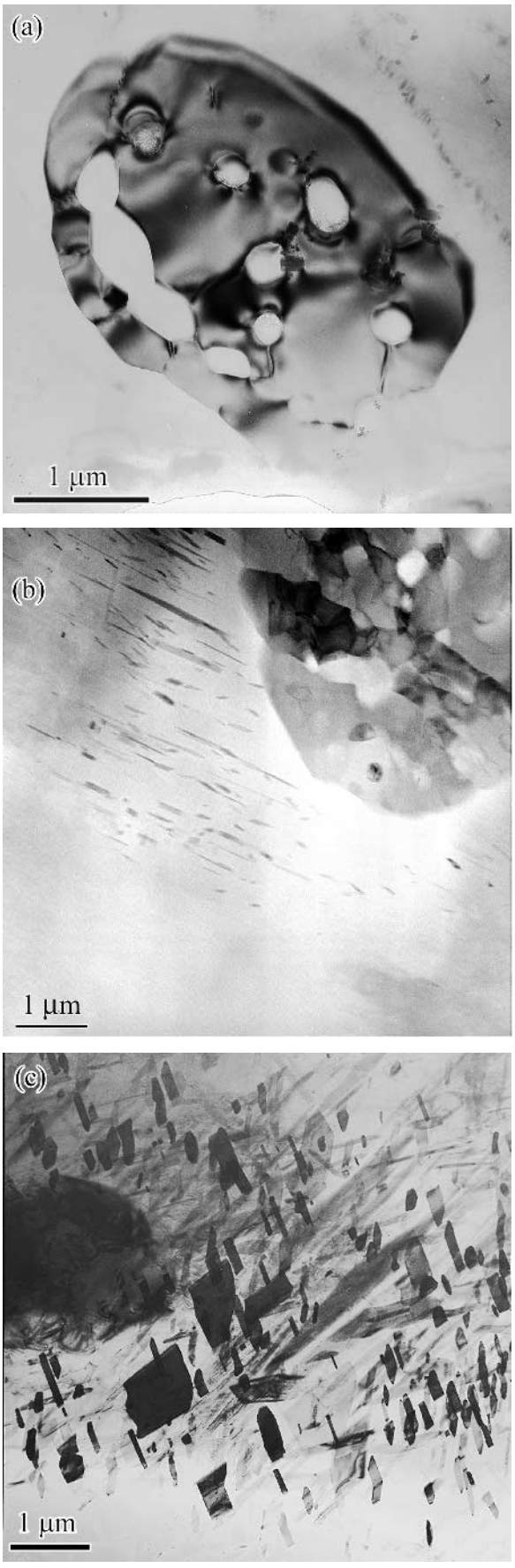


Fig. 4—$Mg_{17}Al_{12}$ particles in the LPDC sample.

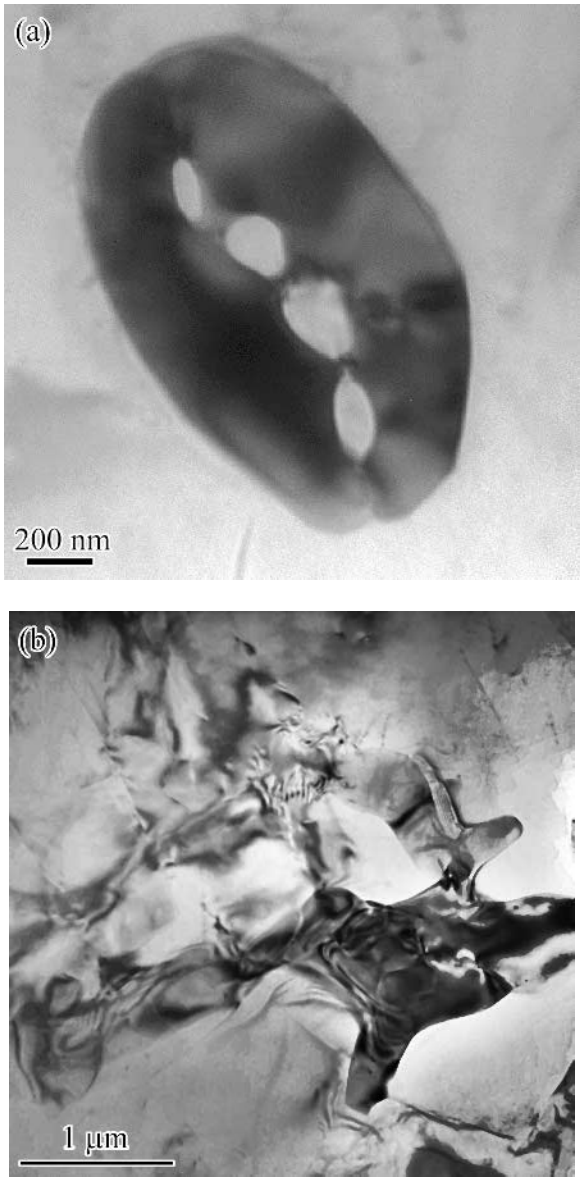


Fig. 5—$Mg_{17}Al_{12}$ particles in the HPDC sample.

the EDS data if the precipitates are assumed to be of a binary Al-Mn intermetallic phase and the entire Mg signal comes from the matrix. Thus, we have assumed that the $\alpha$(Mg) matrix contains 3 pct Al and that the rest of the Al is bound with Mn in the precipitate. Such an approach leads to surprisingly consistent results, despite different proportions of relative volumes of particles and matrix in different measurements causing a large scatter of raw uncorrected data. Analyses of nanoparticles from three different regions showed their composition to be 62.8 ± 3.1 at. pct Al and 37.2 ± 3.1 at. pct Mn. This suggests that the precipitates are still of the same $Al_8Mn_5$ phase. Only two small regions were found with a few Al-Mn particles near $Mg_{17}Al_{12}$ nanoprecipitates (Figure 11). The Al-Mn precipitates in these regions show a different chemical composition. Quantitative analyses of such particles using the approach described earlier have shown their composition to be 79.2 ± 1.7 at. pct Al and 20.8 ± 1.7 at. pct Mn. This corresponds to an "$Al_4Mn$" compound. The chemical formula is written in quotation marks because

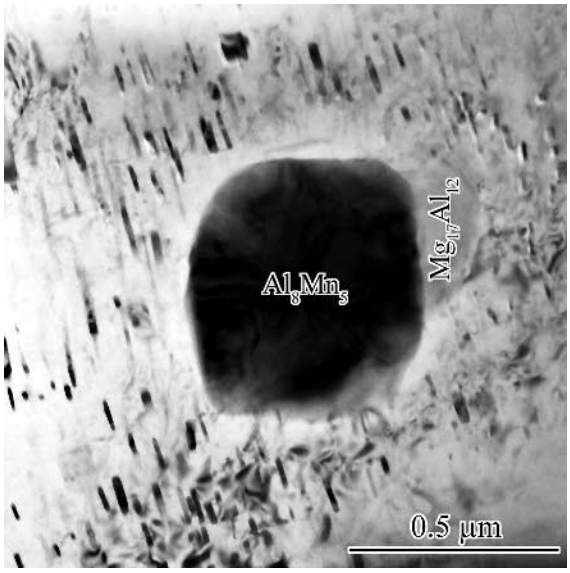


Fig. 6—Intermetallic particles in the HPDC sample after creep for 130 hours at 125 °C. The coarse particles are eutectic constituents. The fine elongated precipitates are $Mg_{17}Al_{12}$.

there actually exist two equilibrium hexagonal phases with close stoichiometry: the $\lambda$ phase with ~17 to 19 at. pct Mn and the $\mu$ phase with ~19 to 21 at. pct Mn.[14,15,16] The precipitates observed in this case are probably of the $\mu$ phase.

## IV. PHASE TRANSFORMATIONS DURING PRESSURE DIE CASTING OF MAGNESIUM ALLOY

Let us consider phase transformations that could lead to the formation of phases observed in the present study. Even though solidification of the alloy during pressure die casting is apparently a nonequilibrium crystallization process, it is instructive to start consideration from equilibrium phases and transformations. The Mg-Al-Mn ternary-phase diagram is not known in great detail,[15] but some features near the Mg corner have already been determined. Thus, it was established several decades ago[20,21,22] that equilibrium phases at room temperature in Mg alloys with 2 to 9 pct Al and less than 1 pct Mn are $\alpha$(Mg) solid solution, $Mg_{17}Al_{12}$, and $Al_8Mn_5$. Also, from the results of experiments on rapidly quenched melt droplets,[22] one can deduce the phase composition at the low- and high-pressure die-casting temperatures. Thus, by extrapolating their data on the solubility of Mn in melts of Mg-4 pct Al-Mn, we obtain the maximum solubility of ~0.3 wt pct Mn at 690 °C and ~0.7 wt pct Mn at 725 °C. An additional amount of Al in this case (5 *vs* 4 pct) leads to somewhat reduced solubility of Mn in the melt, but the difference is not large for the compositions with 4 and 5 pct Al.[22] So, this analysis indicates that, given the Mn concentration in the samples (Table I), the alloy is fully melted at 725 °C (LPDC sample), while the melt should contain inclusions of the $Al_8Mn_5$ phase at 690 °C (HPDC sample). The solubility of Mn in the melt decreases rapidly with decreasing temperature[22] and, hence, new particles of $Al_8Mn_5$ appear during cooling. Since the cooling after the high-pressure die-casting process is very fast, very few such particles can precipitate from the melt. On the other hand, cooling after the low-pressure die-casting process is slower and starts from a higher temperature. Thus, one can expect to find some $Al_8Mn_5$ particles formed on cooling in the LPDC sample. This is also consistent with the microstructural observations of Simensen *et al.,*[22] that inclusions in the melt have regular shapes, while particles formed during cooling have irregular shapes (compare with our observations (Figure 7)).

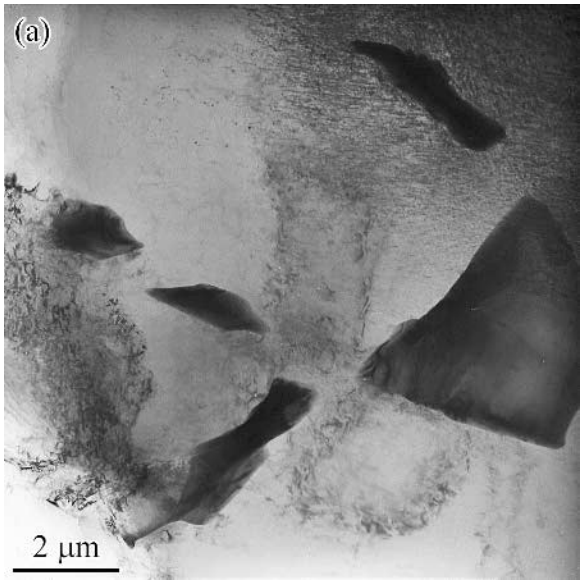


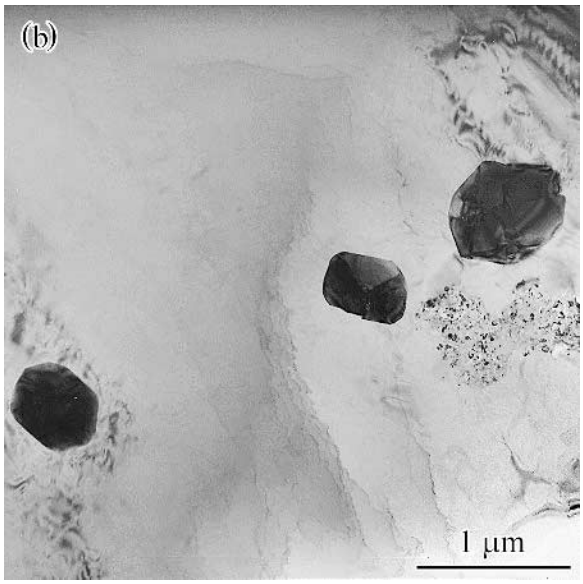


Fig. 7—Coarse $Al_8Mn_5$ inclusions in the (*a*) LPDC and (*b*) HPDC samples.

During further cooling, the $\alpha$(Mg) solid solution begins to crystallize. As usual, the first crystallized volumes (dendrite centers in the LPDC sample and solidification-cell centers in the HPDC sample) have a reduced solute concentration, while the regions at the periphery are supersaturated. Eventually, the solute concentration in the remaining liquid pockets becomes so high that the melt undergoes eutectic transformation. Microstructural observations allow determination of what eutectic constituents are present.

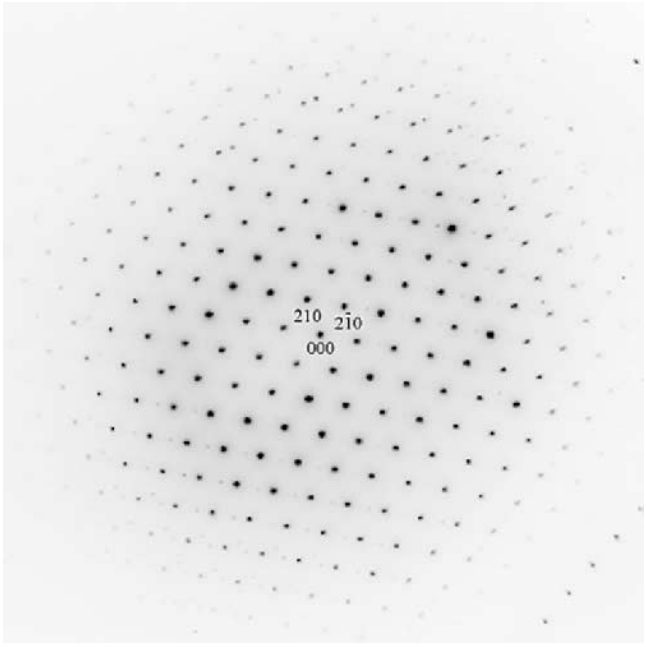


Fig. 8—Selected-area electron diffraction pattern from an individual Al-Mn particle matching $[001]_{Al8Mn5}$.

One can notice from Figures 2 and 3 that, while some $Al_8Mn_5$ inclusions are within the initially crystallized $\alpha$(Mg) regions and were obviously present before the solid-solution crystallization began, the majority of the $Al_8Mn_5$ particles are present in the outer regions. Moreover, such particles have frequently been observed within $\alpha$(Mg)-$Mg_{17}Al_{12}$ eutectic islands (Figure 12). Notice also the coexistence of the $Mg_{17}Al_{12}$ and $Al_8Mn_5$ particles in Figure 6. This suggests that we deal with a ternary eutectic in the alloy. Even though no mention has been found in the literature about the $\alpha$(Mg)-$Mg_{17}Al_{12}$–$Al_8Mn_5$ ternary eutectic, the microstructures observed in the present study seem to be consistent with this interpretation. A very small volume fraction of $Al_8Mn_5$ in this case is not a contradiction—it is quite common for the eutectic point to be near the lower-melting-point constituent when the other constituent has a much higher melting temperature. Note that the $Al_8Mn_5$ particles within eutectic regions, again, have regular shapes, unlike those formed in the melt during cooling.

Observations of eutectic inclusions without $Al_8Mn_5$ particles (Figures 4 and 5) could be interpreted such that a binary eutectic is also present in the samples. Obviously, the phase-diagram boundary between the binary and ternary eutectics depends on the Mn concentration, and composition variations within the sample could be large enough so that both the binary and ternary eutectics could be observed at different locations. On the other hand, due to the low volume fraction of $Al_8Mn_5$ in the ternary eutectic, particles of this phase may simply not be encountered in arbitrary sections in the TEM foils—the dual-phase mixtures seen in Figures 4 and 5 might, in fact, be tri-phase formations in three dimensions.

When solidification is complete, the alloy contains an $\alpha$(Mg) solid solution with a variable concentration of solutes, primary inclusions of $Al_8Mn_5$ (present in the initial melt in the HPDC sample and formed during cooling of the melt in the LPDC sample), and eutectic constituent particles of

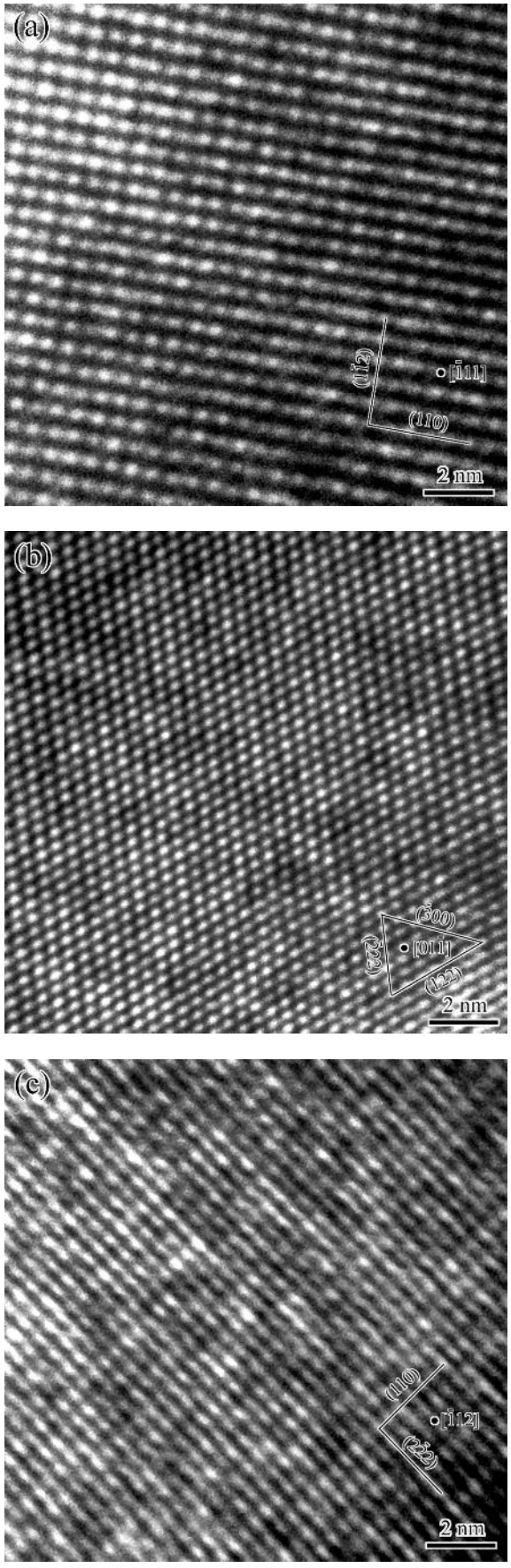


Fig. 9—High-resolution lattice images of $Al_8Mn_5$.

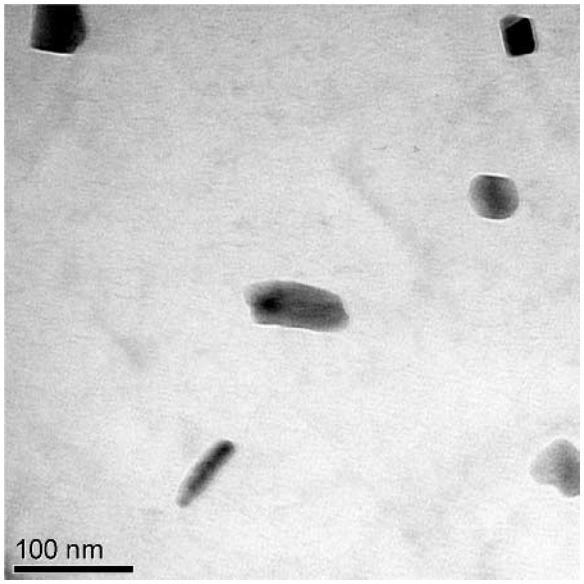


Fig. 10—Al-Mn nanoparticles in the LPDC sample.

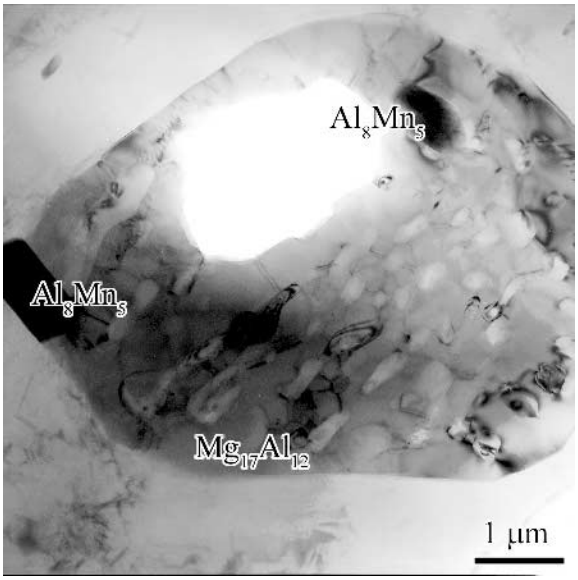


Fig. 12—Eutectic island in the LPDC sample containing both $Mg_{17}Al_{12}$ and $Al_8Mn_5$.

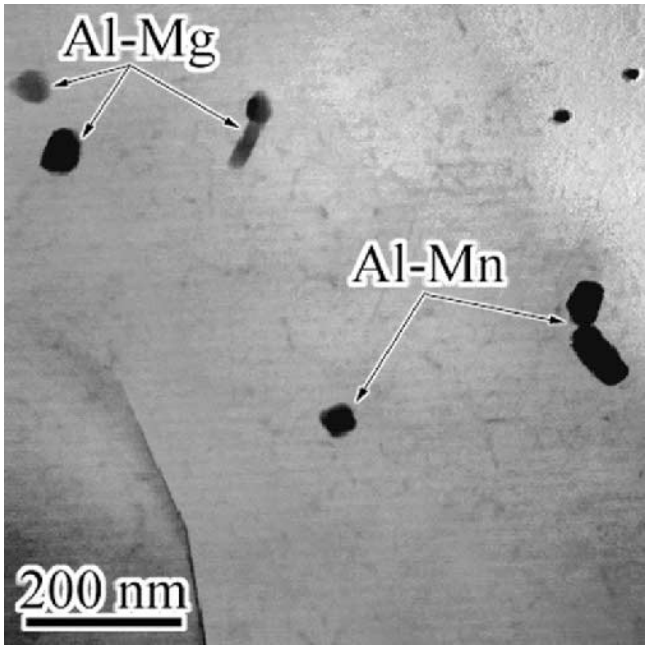


Fig. 11—Nanosized precipitates of different intermetallic phases in the same region.

$Mg_{17}Al_{12}$ and $Al_8Mn_5$. Further cooling to room temperature leads to precipitation of ultrafine particles of $Mg_{17}Al_{12}$ and $Al_8Mn_5$ in the areas of supersaturated solid solution in the LPDC sample. As mentioned in the previous section, on a couple of occasions, nanoparticles of the $Al_4Mn$ $\mu$ phase have been found, which may have formed because of local compositional variations. Several X-ray studies[20,21,22] show that different stable and metastable binary Al-Mn compounds could precipitate in small amounts in cast Mg-Al-Mn alloys. Fast cooling of the HPDC sample actually amounts to quenching, and no precipitation in the solid state occurs. However, as mentioned previously, deformation at elevated temperature causes precipitation of $Mg_{17}Al_{12}$ particles in the HPDC sample (Figure 6). At the same time, no nanoprecipitates of the $Al_8Mn_5$ phase have been found in this sample. In addition to the possibility that, due to the very inhomogeneous microstructure, such precipitates were not present in the areas examined in the TEM, another explanation could be put forth. According to results of Simensen *et al.*[22] discussed earlier, the concentration of Mn in the melt at 725 °C (LPDC sample) is much higher than that at 690 °C (HPDC sample). Even though the average Mn content is somewhat lower in the LPDC sample, and the cooling rate is higher for the HPDC sample, eventual supersaturation of the solid solution by Mn could be greater in the LPDC condition, thus creating a greater driving force for precipitation of Al-Mn intermetallic particles. Another factor could be that postsolidification cooling takes place from a higher temperature in the LPDC than in the HPDC sample, because of the higher mold temperature.

## V. SUMMARY

The microstructure of the samples consists of grains of the $\alpha$ solid solution, which is primarily Mg with dissolved Al, and nonuniformly distributed particles of the intermetallic phases $Mg_{17}Al_{12}$ and $Al_8Mn_5$. Particles of the same phase exhibit different dimensions and morphologies, depending on their formation conditions. $Mg_{17}Al_{12}$ is present as both coarse particles (eutectic constituent) and fine precipitates formed from supersaturated solid solution. $Al_8Mn_5$ is also found as eutectic constituent particles and, in the LPDC condition, fine precipitates. In addition, there are coarse primary particles of this phase present in the melt at the HPDC casting temperature and formed from the melt during cooling (mainly in the LPDC sample) before the beginning of solidification of the $\alpha$ solid solution. The presence of a ternary eutectic may have rather serious implications, since this is a low-melting-point microstructural constituent. Obviously, by changing the die-casting and mold temperatures, as well as

the cooling rate, one can obtain different microstructures and intermetallic phase constituents in the alloy and, thus, tailor its properties.

## ACKNOWLEDGMENTS

This research was funded by the Climate Change Technology and Innovation Initiative and the Canadian Lightweight Materials Research Initiative (CLiMRI), Government of Canada. Mr. Mike Evans and Gibbs Die Casting Corporation are gratefully acknowledged for providing HPDC samples. The authors also thank Mr. Claude Marchand and Ms. Pei Liu for their help with metallography and Ms. Catherine Bibby for preparing TEM samples.

## REFERENCES

1. *Magnesium Alloys and Their Applications,* Proc. Int. Conf., Munich, 2000, K.U. Kainer, ed., Wiley, New York, NY, 2000.
2. *Magnesium Technology 2000,* Proc. Symp. 2000 TMS Annual Meeting, Nashville, TN, 2000, H.I. Kaplan, J. Hyrn, and B. Clow, eds., TMS, Warrendale, PA, 2000.
3. *Magnesium Technology 2001,* Proc. Symp. 2001 TMS Annual Meeting, New Orleans, LA, 2001, J. Hryn, ed., TMS, Warrendale, PA.
4. *Magnesium Technology 2002,* Proc. Symp. 2002 TMS Annual Meeting, Seattle, WA, 2002, H. Kaplan, ed., TMS, Warrendale, PA, 2002.
5. *Magnesium Technology 2003,* Proc. Symp. 2003 TMS Annual Meeting, San Diego, CA, 2003, H. Kaplan, ed., TMS, Warrendale, PA, 2003.
6. *Magnesium Technology 2004,* Proc. Symp. 2004 TMS Annual Meeting, Charlotte, NC, 2004, A.A. Luo, ed., TMS, Warrendale, PA.
7. *Magnesium: Proc. 6th Int. Conf. Magnesium Alloys and Their Applications,* Wolfsburg, Germany, 2003, K.U. Kainer, ed., Wiley, New York, NY, 2003.
8. *61st Annual World Magnesium Conf.,* New Orleans, LA, May 9-12, 2004.
9. S.R. Agnew, S. Viswanathan, E.A. Payzant, Q. Han, K.C. Liu, and E.A. Kenik: *Magnesium Alloys and Their Applications,* Proc. Int. Conf., Munich, 2000, K.U. Kainer, ed., Wiley, New York, NY, 2000, pp. 687-92.
10. K.Y. Sohn, J.W. Jones, and J.A. Allison: in *Magnesium Technology 2000,* Proc. Symp. 2000 TMS Annual Meeting, Nashville, TN, 2000, H.I. Kaplan, J. Hyrn, and B. Clow, eds., TMS, Warrendale, PA, pp. 271-78.
11. R.M. Wang, A. Eliezer, and E.M. Gutman: *Mater. Sci. Eng.,* 2003, vol. A355, pp. 201-07.
12. M.T. Perez-Prado, J.A. del Valle, J.M. Contreras, and O.A. Ruano: *Scripta Mater.,* 2004, vol. 50, pp. 661-65.
13. G. Pettersen, H. Westengen, R. Høier, and O. Lohne: *Mater. Sci. Eng.,* 1996, vol. A207, pp. 115-20.
14. T.B. Massalski: *Binary Alloy Phase Diagrams,* ASM INTERNATIONAL, Metals Park, OH, 1990, pp. 169-74 and 2520-21.
15. *Alloy Phase Diagrams,* vol. 3, *ASM Handbook,* ASM INTERNATIONAL, Metals Park, OH, 1991, pp. 2-48, 2-280, and 3-17.
16. W.G. Moffatt: *The Handbook of Binary Phase Diagrams,* Genium Publ., Schenectady, NY, 1988.
17. S. Xu, J. Li, V.Y. Gertsman, J.P. Thomson, and M. Sahoo: *Proc. Int. Symp. on Light Metals and Metal Matrix Composites,* 43rd Annual Conf. of Metallurgists of CIM (COM 2004), Hamilton, ON, 2004, D. Gallienne and R. Ghomashchi, eds., TMS-CIM, Montreal, QC, pp. 41-55.
18. S. Xu, V.Y. Gertsman, J. Li, J.P. Thomson, and M. Sahoo: "Microstructural Investigation on As-Cast, Deformed and Aged Magnesium Alloy AM50," Report CANMET-MTL 2004-7(TR), Ottawa, ON, 2004.
19. H.-G. Messner and K. Schubert: *Z. Metallkund.,* 1965, vol. 56, pp. 523-30.
20. N.F. Lashko, G.I. Morozova, I.Y. Mukhina, and M.A. Timonova: *Russ. Metall. (Metally),* 1971, No. 4, pp. 138-41.
21. I.Y. Mukhina, M.A. Timonova, and G.I. Spiryakina: *Russ. Metall. (Metally),* 1973, No. 6, pp. 123-26.
22. C.J. Simensen, B.C. Oberländer, J. Svalestuen, and A. Thorvaldsen: *Z. Metallkd.,* 1988, vol. 79, pp. 537-40 and 696-99.